BMC Chemistry

RESEARCH Open Access

Docking-based virtual screening of BRD4 (BD1) inhibitors: assessment of docking methods, scoring functions and in silico molecular properties

Junmin Dong[1] and Xiaohua Hao[1*]

Abstract

To enhance the accuracy of virtual screening for bromodomain-containing protein 4 (BRD4) inhibitors, two docking protocols and seven scoring functions were compared. A total of 73 crystal structures of BRD4 (BD1) complexes were selected for analysis. Firstly, docking was carried out using both the LibDock and CDOCKER methods. The CDOCKER protocol was shown to be more effective based on the root mean square deviation (RMSD) values (in Å) between the docking positions and the co-crystal structures, achieving a docking accuracy rate of 86.3%. Then, among the various scoring functions (LigScore1, LigScore2, PLP1, PLP2, PMF, PMF04 and Ludi3), PMF showed the highest correlation with inhibition constants ($r^2 = 0.614$), while Ludi3 scored lowest ($r^2 = 0.266$). Finally, using ligand descriptors from PubChem, a strong correlation ($r^2 > 0.5$) with inhibition constants for heavy atom count was found. Based on these comprehensive evaluations, the PMF scoring function emerged as the best tool for docking-based virtual screening of potential BRD4 (BD1) inhibitors. And the correlation between molecular properties and BRD4 (BD1) ligands also provided information for future design strategies.

Keywords BRD4 (BD1), Inhibitor, Docking, Scoring function, Molecular property

Introduction

The process of discovering drugs is costly and time-consuming, often requiring 10–15 years before a drug reaches the commercial market [1]. Owing to their cost-effectiveness and the ability to rapidly produce results, various computer-aided methods have been suggested and implemented in the process of lead discovery and drug design [2]. Among these methods, virtual screening (VS) has emerged as a crucial computer aided drug design (CADD) application, which can rapidly identify potential molecules from millions of compounds [3]. There are two main virtual screening approaches: ligand-based virtual screening (LBVS) and structure-based virtual screening (SBVS) [4]. LBVS relies on known information about ligands, such as structures, chemical properties or their combination, to predict binding force based on the premise that similar ligands are likely to bind to similar targets [5]. SBVS commonly employs molecular docking, initiating with the generation of 3D conformations. As documented in various research articles, innovative ligands have been identified for specific drug targets through the application of molecular docking technology [6–10]. Generally speaking, the evaluation of molecular docking results is traditionally carried

*Correspondence:
Xiaohua Hao
hxh3949@bjsjth.cn
[1]Phase I Clinical Trial Center, Beijing Shijitan Hospital, Capital Medical University, Beijing 100038, China

out using classical scoring functions to gauge their potential effectiveness [11]. Primary challenges faced by all docking methods encompass dealing with the flexibility of molecules and providing an accurate representation of actual binding interactions. Undoubtedly, the precision of these scoring functions has a significant impact on the outcome and reliability of molecular docking studies and has been the subject of extensive research [12, 13].

BRD4 recognizes and binds to acetylated lysine residues on histones, recruiting chromatin regulatory proteins and transcription factors [14, 15]. It regulates various cellular processes such as cell cycle, proliferation, and apoptosis, thereby controlling inflammation, viral infections, cancer and others [16]. It contains two *N*-terminal bromodomains (BD1 and BD2), an ET domain and a *C*-terminal domain (CTD) [17]. The two bromodomains of the BRD4 protein share over 90% sequence identity and both contain a conserved KAc binding pocket [18]. Specific residues in the BD1 binding pocket include Gln85, Lys141, Asp144, and Ile146, while specific residues in BD2 include Lys374, Pro430, His433, and Val435 [19]. The BD1 binding pocket is larger and exhibits changes in polarity and hydrophobicity compared to BD2 [20]. Studies have shown that both BD1 and BD2 contribute to the rapid induction of gene expression following inflammatory stimuli. Besides, BD1 plays a critical role in steady-state gene expression [21]. BRD4 (BD1) inhibitors and pan-BRD4 inhibitors exhibit similar effects in tumor models, while BRD4 (BD2) inhibitors have limited efficacy in tumors and are only effective in models of inflammation and autoimmune diseases [22]. Clinical application of pan-BRD4 inhibitors has shown side effects such as thrombocytopenia, testicular toxicity, and gastrointestinal toxicity [23, 24]. Consequently, development of low-toxicity BD1 selective inhibitors is of great significance for reducing drug side effects [25].

Recent studies have highlighted advancements in the application of computational methods in the discovery of novel inhibitors targeting BRD4. For instance, Zhong et al. successfully identified a promising BRD4 inhibitory compound, SQ-1, which exhibited an IC_{50} value of 676 nM, using SBVS strategies [26]. In another study, the SuperDRUG2 database, which comprised more than 4,600 pharmacologically active compounds, underwent a virtual screening process against the BRD4 (BD1) binding site, employing both molecular docking and molecular dynamics simulations to evaluate interactions [27]. Furthermore, Allen et al. developed a virtual screening workflow aimed at identifying potent inhibitors of BRD4 (BD1), resulting in the identification of *N*-[3-(2-oxo-pyrrolidinyl) phenyl]-benzenesulfonamide derivatives as potential lead compounds [28].

In our research, the primary objective was to identify novel inhibitors for BRD4 (BD1) through the application of docking-based virtual screening techniques. Hence, before initiating a large-scale screening of the database, we initially evaluated two distinct molecular docking methodologies along with seven different scoring functions to ensure the reliability and effectiveness of the screening process prior [29]. By correlating these in silico molecular properties with the inhibition potency, we aimed not only to identify potential inhibitory compounds but also to gain insights into the molecular structures that contributed to effective BRD4 (BD1) inhibitions. This preparatory phase was crucial for optimizing our screening protocol to efficiently identify promising BRD4 (BD1) inhibitors.

Methods

Crystal structures of BRD4 (BD1) complexes

The RCSB Protein Data Bank (https://www.rcsb.org/) serves as the US data center for the global protein database. This database stores 3D structural data of large biological molecules, which are crucial for research in areas like fundamental biology, health, energy, and biotechnology [30]. In this work, 177 crystal structures of human BRD4 (BD1) complexes were downloaded from this website. Considering the resolution of crystal structure (≤ 2.5 Å), biological activities (expressed as IC_{50} or Ki values), diversity of ligand structures, completeness of protein chain structures and others, we ultimately retained 73 complexes for further analysis. Table S1 provided detailed information about them. In cases where the structures were dimers or tetramers, only monomer A was chosen for subsequent analysis [31]. The duplicate protein chains were deleted, and the corresponding ligand was extracted from the crystal structure and saved for future use. The Protein Preparation module in the Discovery Studio 2019 (hereinafter referred to "DS 2019") software was used to solve potential problems in the protein structure. By inputting protein into module, tasks such as inserting missing atoms in incomplete residues, modeling missing loop regions, deleting alternate or disorder conformations, standardizing atom names, and generating the protonation state at pH 7.0 were performed [32, 33].

To more effectively analyze the differences across the 73 BRD4 (BD1) crystal structures, we aligned all structures utilizing the Align Sequences and Structures module within the DS 2019 software. The overlay of the crystal structures and comparison of amino acid sequences were shown in Fig. 1. High consistency among the 73 crystal structures, including a well-defined binding pocket was revealed. Owing to the induced-fit theory, protein structures underwent conformational changes upon ligand binding. Consequently, minor conformational variations were observed across the 73 co-crystalized structures.

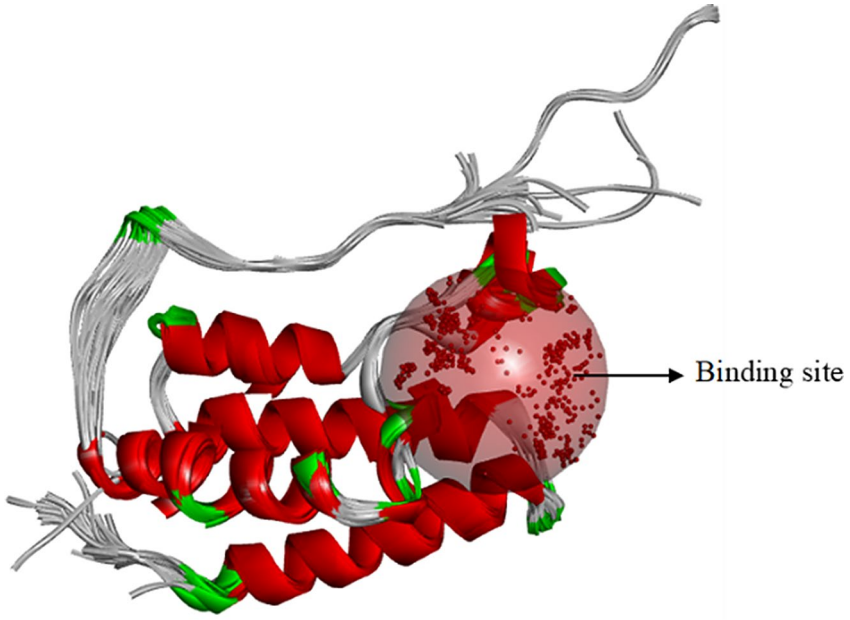

Fig. 1 Overlay of 73 BRD4 (BD1) crystal structures. The red sphere represented binding site. The red dot in binding site represented water molecules

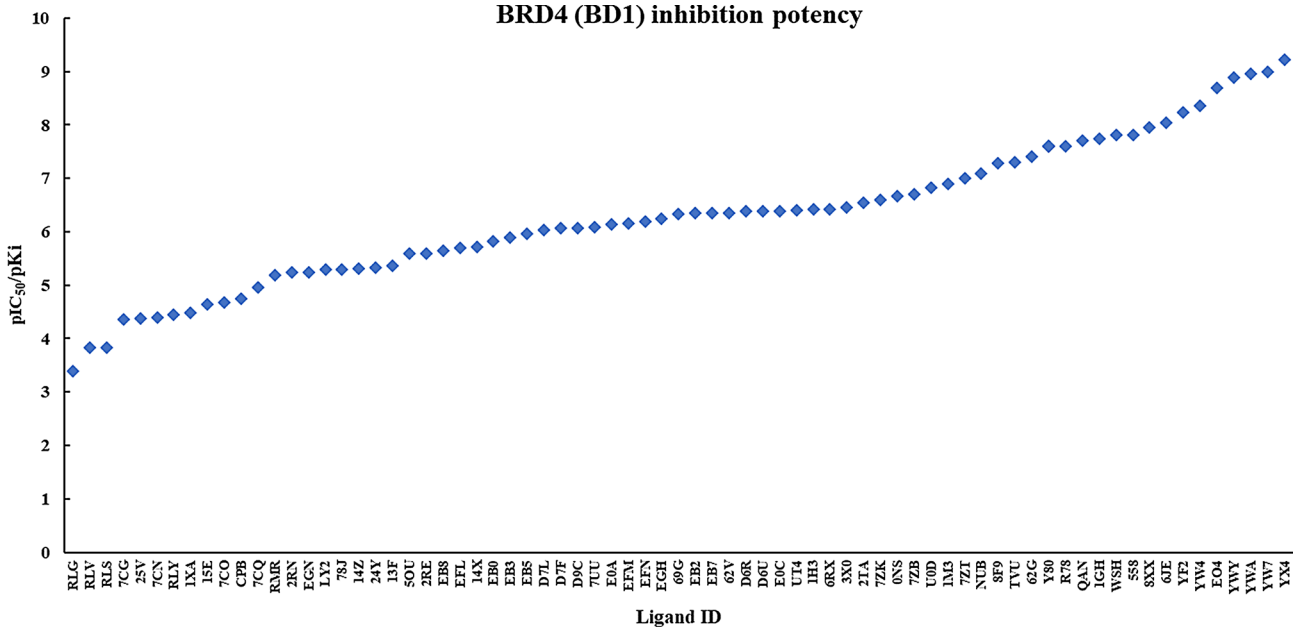

Fig. 2 Distribution of pIC_{50} (pKi) values of the studied ligands. Every ligand was labelled with an alphanumeric code sourced from the PDB. The X-axis represented the ligand ID. The Y-axis represented their pIC_{50} (pKi) values

Preparation of ligands

The biology activities of 73 inhibitors in the crystal structures of BRD4 (BD1) complexes were obtained from literatures (Table S2). And all of them were expressed as IC_{50} values, except for 6RX (PDB ID: 5KDH) expressed as Ki value [34]. The IC_{50} or Ki values spanned seven orders of magnitude (10^{-10}-10^{-4} M) and were further converted into pIC_{50} or pKi using the formula pIC_{50}= -log IC_{50} (pKi= -log Ki). Distribution of pIC_{50} (pKi) values was shown in Fig. 2. Prior to docking, the ligand structures from the BRD4 (BD1) complexes were saved in a separate SD file, and the CHARMm force field was applied.

Molecular docking

Molecular docking plays a vital role in drug discovery, enabling the prediction of how specific molecules will bind to a target. This research utilized two docking methods, LibDock and CDOCKER within DS 2019, to

replicate the binding positions of ligands found in crystal structures. LibDock used a grid placed within the binding site and probed to calculate hotspots for the protein. It was a rigid-based docking module [35]. The CDOCKER module employed the CHARMm flexible docking program, in which, the receptor remained fixed, and the ligands were permitted flexibility during refinement [36]. The accuracy of the docking process was evaluated using the root mean square deviation (RMSD) values (in Å) between the optimal redocked positions of the ligands and their conformations in co-crystal structures.

The ligand YF2 (PDB ID: 6P05) with the pIC_{50} value of 9.23 was chosen to define the active site and the radius of the spherical box was set to 9 Å [37]. Of note, water molecules in active site were kept in their original state because they could stabilize a complex by acting as a bridge for hydrogen bonds [38–41]. In the LibDock module, conformations were generated using the Best method. A limit of 255 maximum conformations was established, along with an energy threshold of 20 $kcal{\cdot}mol^{-1}$, to produce a set of low-energy conformations for each ligand. The setting for Max Hits to Save was configured to 1, while all other parameters were left at their default values.

In the CDOCKER module, the Top Hits was set to 1, with a Pose Cluster Radius defined at 0.5, while the rest of the settings remained at their default values. This configuration ensured that only the best docking pose for each molecule was noted and preserved for additional examination. These 73 active molecules were then re-docked into the active site of BRD4 (BD1), followed by the calculation of RMSD values. For the purpose of virtual screening, RMSD values at or below 2.0 Å were considered satisfactory [42]. Consequently, in this study, docking results yielding RMSD values of 2.0 Å or less were deemed successful, whereas those with RMSD values exceeding 2.0 Å were regarded as unsuccessful.

Scoring functions

The scoring of ligands was conducted via the Score Ligand Poses module in DS 2019 software. The utilized scoring functions were LigScore1, LigScore2, PLP1, PLP2, PMF, PMF04 and Ludi Energy Estimate 3 (Ludi3). The scores were reported as positive values, where higher scores denoted stronger binding affinity. Correlation was then established between the score of each ligand and its corresponding pIC_{50} (pKi) value.

In silico molecular properties of ligands

PubChem database (https://pubchem.ncbi.nlm.nih.gov/) is the most comprehensive source of chemical data freely accessible to users worldwide. It contains information on the chemical structures, bioactivity, health and safety data, spectra data, and other relevant chemical information [43]. In this study, the database was utilized to analyze in silico molecular properties for ligands obtained from BRD4 (BD1) complexes. Seven molecular properties included complexity, hydrogen bond acceptor count, hydrogen bond donor count, molecular weight, rotatable bond count, topological polar surface area and total number of heavy atoms were collected. These descriptors were detailed in the Computed Properties section, which fell under the Chemical and Physical Properties heading. In addition, considering the π-π or cation-π interactions formed between the sp^2-hybridized atoms in the ligand and amino acid residues during docking, three additional descriptors were introduced: the total count of sp^2-hybridized carbons in the ligand, their proportion, and the total atom count.

Molecular dynamic simulation

To investigate the stability of interactions between BRD4 (BD1) with inhibitors, molecular dynamics (MD) simulation was conducted using GROMACS 2018 software [44]. The CHARMM36 force field was utilized to construct the topology of the BRD4 protein [45]. Ligand topology and coordinates were devised through the CGenFF server (https://cgenff.com/). A 10 Å cubical box was constructed, and the simple point charge water model (SPC216) was utilized for solvation purposes [46]. Charge neutrality was then achieved by the addition of appropriate Na^+ and Cl^- ions using the genion tool. Subsequently, an energy minimization process was carried out by applying the steepest descent method, followed by the implementation of positional restraints on the ligands [47]. The systems underwent equilibration in both the NVT (constant number of particles, volume, and temperature) ensemble for 500 ps and the NPT (constant number of particles, pressure, and temperature) ensemble for 1000 ps, sustaining conditions at 300 K and an atmospheric pressure of 1.0 bar. Finally, 30 ns MD simulation was performed for each system.

Results and discussions

Assessment of docking methods

In the virtual screening process, effectively docking ligands to the active site is a crucial step. This study employed the Libdock and CDOCKER programs to determine the most effective docking technique for BRD4 (BD1) while assessing how accurately they predicted the ligand-binding positions. For this purpose, 73 known BRD4 (BD1) inhibitors were redocked into their respective binding pockets. Only the highest-scoring redocked pose for each ligand was selected to represent its potential active conformation. The RMSD values between top-scoring redocked poses and the conformations in co-crystal structures were calculated and presented in Table 1. The evaluation results revealed that the number

Table 1 RMSD values (in Å) between top-scoring redocked poses of ligands and the conformations in co-crystal structures

No.	PDB ID	Ligand ID	RMSD		No.	PDB ID	Ligand ID	RMSD	
			Libdock	CDOCKER				Libdock	CDOCKER
1	7MCF	YX4	0.9047	0.8375	38	6G0F	EGH	4.5449	0.8143
2	5S9Q	YW7	0.8704	0.6155	39	5Z1T	EFN	3.3083	1.7072
3	5S9R	YWA	1.7645	0.6718	40	5Z1S	EFM	3.5639	1.0526
4	7MCE	YWY	0.8682	1.4496	41	5CY9	E0A	3.4178	0.5237
5	6C7R	EO4	1.0087	0.6521	42	5WUU	7UU	1.8799	0.3224
6	5S9P	YW4	1.6680	0.6704	43	6KEJ	D7F	1.7758	0.4833
7	6P05	YF2	0.5825	0.3266	44	6KEC	D9C	0.5505	5.7613
8	5WMD	6JE	6.9327	7.6078	45	6KEK	D7L	0.7637	0.2782
9	5YOU	8XX	0.7065	0.2930	46	5CRM	EB5	0.3751	0.6909
10	4Z1Q	558	0.7620	0.6448	47	5CQT	EB3	0.5948	1.2743
11	2YEL	WSH	0.5878	0.3512	48	5CP5	EB0	0.3553	4.0236
12	3ZYU	1GH	1.0782	0.4566	49	4HBX	14X	0.8503	0.7749
13	6Z7L	QAN	0.4772	0.8155	50	5Z1R	EFL	6.3200	0.3390
14	4O74	R78	3.0226	1.1615	51	5CS8	EB8	2.4308	0.2646
15	4YH3	Y80	2.0716	0.6580	52	4O77	2RE	3.9245	0.7238
16	5HLS	62G	5.4749	1.5317	53	5EIS	5OU	0.5423	3.1488
17	4UIX	TVU	1.9849	1.7496	54	4HBY	13F	3.9149	1.6884
18	5XI2	8F9	0.7532	0.4788	55	4MEP	24Y	0.7725	1.2295
19	6TPY	NUB	0.6216	1.7369	56	4HBW	14Z	0.3210	0.6181
20	7RXS	7ZT	6.5533	0.5719	57	5A85	78J	0.9595	0.6540
21	4O76	1M3	3.9669	7.9171	58	6G0D	LY2	0.7482	0.7854
22	6WGX	U0D	1.2473	0.9142	59	6G0E	EGN	11.0476	6.6573
23	7RXR	7ZB	1.1272	0.7151	60	4O7E	2RN	1.5345	1.4118
24	4E96	0NS	0.5854	2.7171	61	5H21	RMR	6.1577	1.7493
25	7RXT	7ZK	6.5655	2.4482	62	5TI7	7CQ	0.5951	0.3244
26	4PS5	2TA	7.4291	1.6322	63	4O71	CPB	0.4745	0.4255
27	4X2I	3X0	2.3245	0.4755	64	5TI6	7CO	1.0976	0.4608
28	5KDH	6RX	0.7139	0.3961	65	4HBV	15E	0.2979	0.3722
29	4J0S	1H3	0.3800	1.7730	66	4LR6	1XA	0.6977	0.6313
30	6X7D	UT4	1.6201	0.7117	67	6VUJ	RLY	7.4134	0.9243
31	6KEH	D6R	0.3750	0.3513	68	5TI5	7CN	6.0981	0.2574
32	6KEI	D6U	0.7488	1.3213	69	4MEO	25V	1.8122	6.1837
33	5DX4	E0C	7.4228	0.1956	70	5TI3	7CG	2.7128	1.9576
34	5HM0	62V	0.5803	0.2830	71	6VUC	RLS	0.9794	0.3275
35	5CPE	EB2	0.5879	1.1941	72	6VUF	RLV	2.0484	0.8595
36	5CRZ	EB7	1.0030	2.6173	73	6VUB	RLG	0.6289	0.6879
37	5I88	69G	3.0581	0.9608					

of RMSD values greater than 2.0 Å was 25 for the Libdock algorithm and 10 for the CDOCKER algorithm. The accuracy of the former (65.8%) was significantly lower than that of the latter (86.3%). As a result of comparisons and evaluations, CDOCKER program offered superior reliability which was chosen as the docking method for the next phase of our study.

Assessment of scoring functions

73 BRD4 (BD1) complexes had different ligands which encompassed a wide range of inhibition constant values (IC_{50} or Ki). 7 scoring functions were evaluated and the generated scores were compared to the corresponding pIC_{50} (pKi) values of ligands. Correlation analysis was performed with respective pIC_{50} (pKi) values using a linear regression model in GraphPad Prism 9.3.0 software. Detailed calculated scores for various scoring functions could be found in Table S3. Table 2 displayed the correlation coefficients between the kinetic data and the calculated scores for various scoring functions. Figure 3 showed corresponding linear curves.

The slope and the Y-intercept of the regression line for each scoring function suggested the strength and the extent of bias in predictions, respectively. The LigScore1 function had a slope of 0.373, coupled with a Y-intercept of 0.248, while LigScore2 displayed a slightly steeper slope of 0.386 with a considerably higher Y-intercept value of 2.818. Comparatively, PLP1 and PLP2 both

Table 2 Correlation of scores with kinetic data pIC_{50} (pKi) for 73 known inhibitors

Scoring function	Slope*	Y-intercept*	*R* square**	F value	Residuals (D'Agostino-Pearson)	*P* value (D'Agostino-Pearson)	Mean of residuals (%)	SD*** of residuals (%)
LigScore1	0.373 ± 0.07	0.248 ± 0.451	0.285	28.29	16.71	0.0002	-7.121	3.169
LigScore2	0.386 ± 0.041	2.818 ± 0.263	0.557	89.19	6.99	0.030	-0.682	0.969
PLP1	8.999 ± 1.031	26.25 ± 6.628	0.518	76.23	21	< 0.0001	-1.762	1.543
PLP2	8.011 ± 1.056	28.29 ± 6.791	0.448	57.55	21.07	< 0.0001	-1.993	1.630
PMF	10.22 ± 0.962	16.76 ± 6.183	0.614	113.1	2.136	0.344	-1.851	1.796
PMF04	6.279 ± 0.743	-5.165 ± 4.775	0.502	71.51	2.865	0.239	-6.303	3.442
Ludi3	44.43 ± 8.761	292.1 ± 56.34	0.266	25.72	2.01	0.366	-3.120	2.168

* Best-fit value ± SE

** $p < 0.0001$

*** Standard deviation

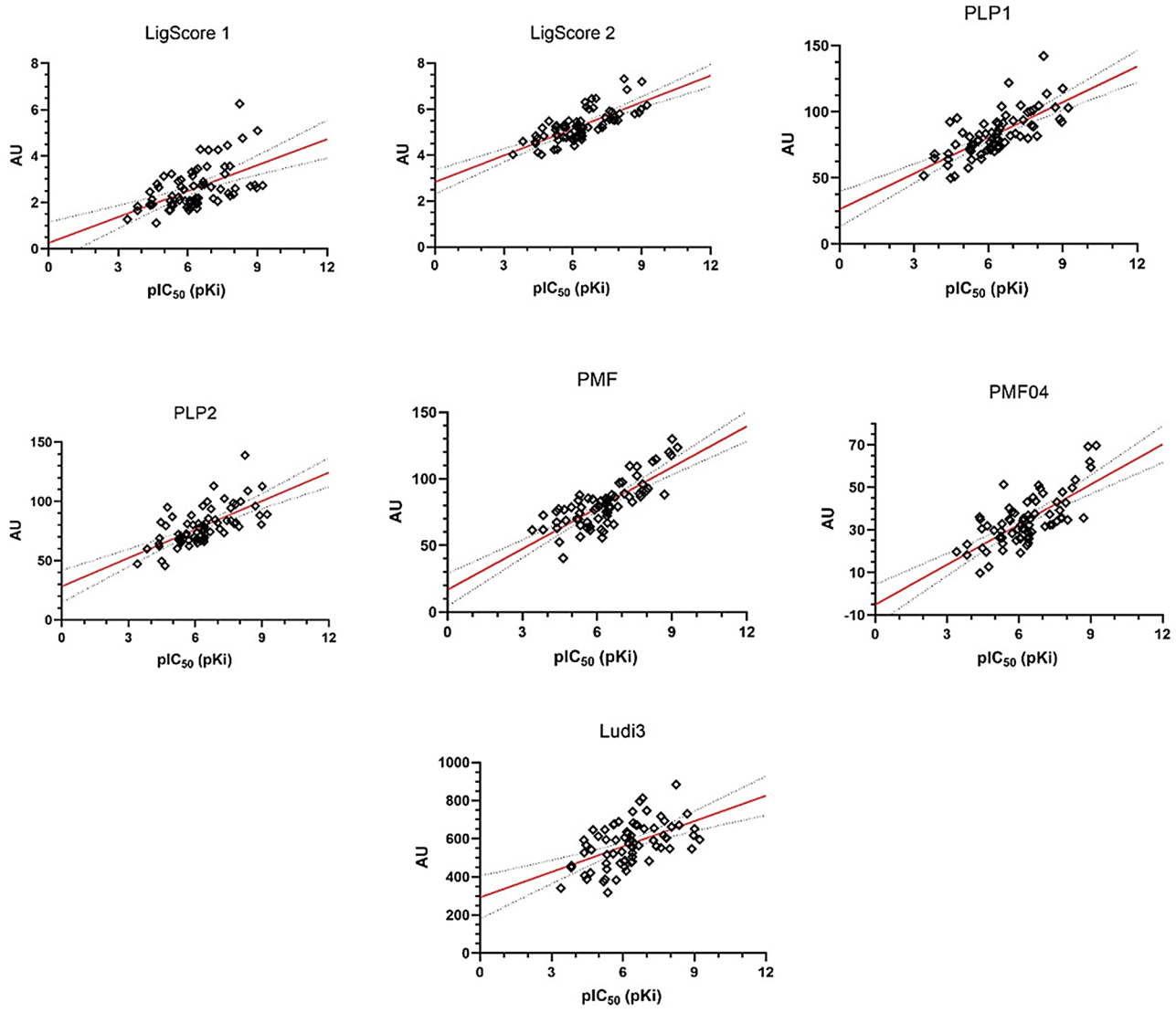

Fig. 3 Linear curves between pIC_{50} (pKi) and calculated scores

exhibited significantly larger slopes, 8.999 and 8.011, respectively, accompanied by sizeable Y-intercept values (PLP1: 26.25, PLP2: 28.29). PMF demonstrated a slope of 10.22 and a Y-intercept of 16.76. PMF04 had a slope of 6.279 and a negative Y-intercept of -5.165. The Ludi 3 scoring function presented with the largest slope among all scoring functions, 44.43, and a Y-intercept of 292.1. At the same time, in the context of predicting molecular affinities, an ordinate standard error (SE) served as a vital indicator, revealing the magnitude of prediction inaccuracies or errors. Specifically, a lower SE value signified a higher precision in the predicted affinity values. In this analysis, the error for the Ligscore2 scoring function was notably low, at 0.263, indicating satisfactory predictive accuracy. This significantly contrasted with the results from other scoring functions like PLP1, PLP2, PMF, and Ludi3, where the errors significantly exceeded 5.

The r-squared (r^2) value in linear regression indicated how well the data fitted the regression line, with values closer to 1 suggesting a better fit. In Fig. 4, r^2 values between predicted and observed binding affinities ranged from 0.266 to 0.614. The PMF scoring function showed the highest r^2 value (0.614), suggesting the best predictive capability within the dataset. Interestingly, despite being developed using a sample size approximately ten times smaller than PMF04, PMF outperformed PMF04. This underscored the utility of smaller, diverse datasets for robust structure-activity insights. LigScore2 followed with an r^2 value of 0.557. Conversely, the Ludi3 scoring function displayed the lowest r^2 value (0.266), which might indicated the least predictive power in this group. F values from the analysis of variance (ANOVA) tests, which assessed the significance of regression models, ranged from 25.72 to 113.1. Higher values indicated the model accounts for a substantial proportion of the variability. In line with the obtained r^2 values, PMF scored the highest F value (113.1), LigScore2 ranked second, while Ludi3 had the lowest (25.72). These results suggested a better statistically significant fit for PMF and Ligscore2 compared to other models.

Fig. 5 presented QQ plots that compared predicted residuals against actual residuals for the scoring functions under analysis. To ensure a fair comparison between scoring functions, all residuals were normalized to percentage values of each score before conducting cross-function residual analysis. This process ensured that differences in absolute scores across functions did not distort the comparison. In this normalized framework, the mean of the residuals, represented as percentages, indicated the average variance from the expected values based on the linear regression model. What's more, the standard error of these normalized residuals indicated how spread out the data points were around the regression line. Analysis of the residuals reflected the differences between observed and predicted binding affinities. The results revealed standard deviation (SD) values ranging from 0.969 to 3.442, with LigScore2 and PMF04 displaying the lowest and highest SD values, respectively. Greater predictive accuracy and consistency were indicated by a lower SD value, while the mean of the residuals varied among scoring functions, suggesting differing levels of systematic bias in their predictions. Specifically, this variation ranged from as low as -0.682 for LigScore2 to -7.121 for LigScore1.

To check normal distribution of residuals, the D'Agostino-Pearson omnibus normality test was performed on the limited dataset. The standard for normality at p value was set less than 0.05. Indeed, among the scoring functions assessed, only PMF, PMF04, and Ludi3 successfully met the criteria of the normality test. Others fell outside the bounds of this standard and hence did not substantiate the normality hypothesis. This

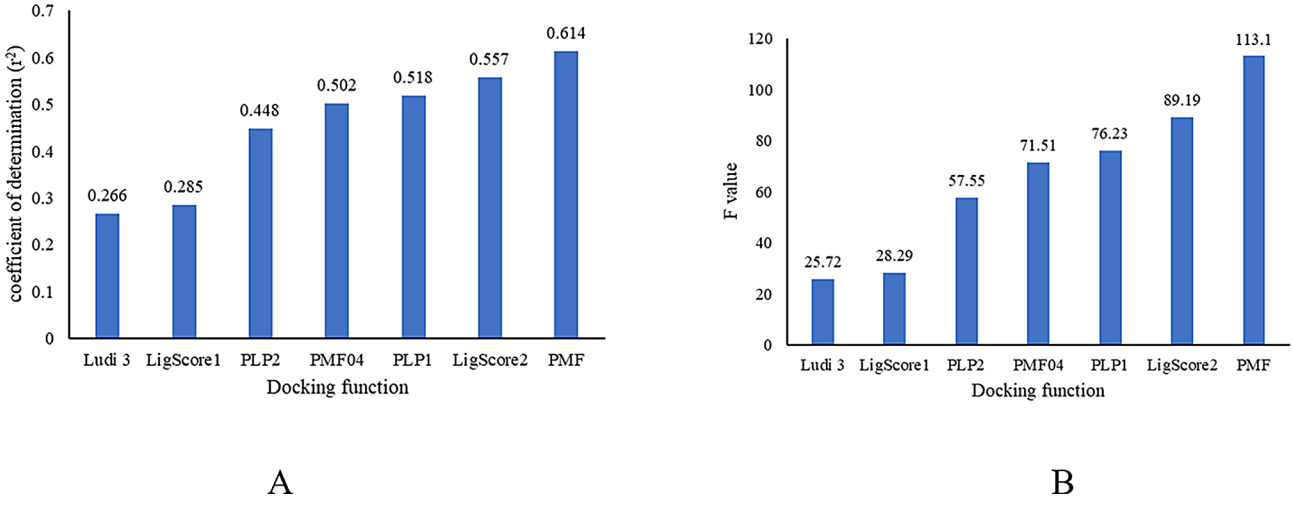

Fig. 4 Ranking of scoring functions based on coefficient of determination (r^2) (**A**) and F value (**B**)

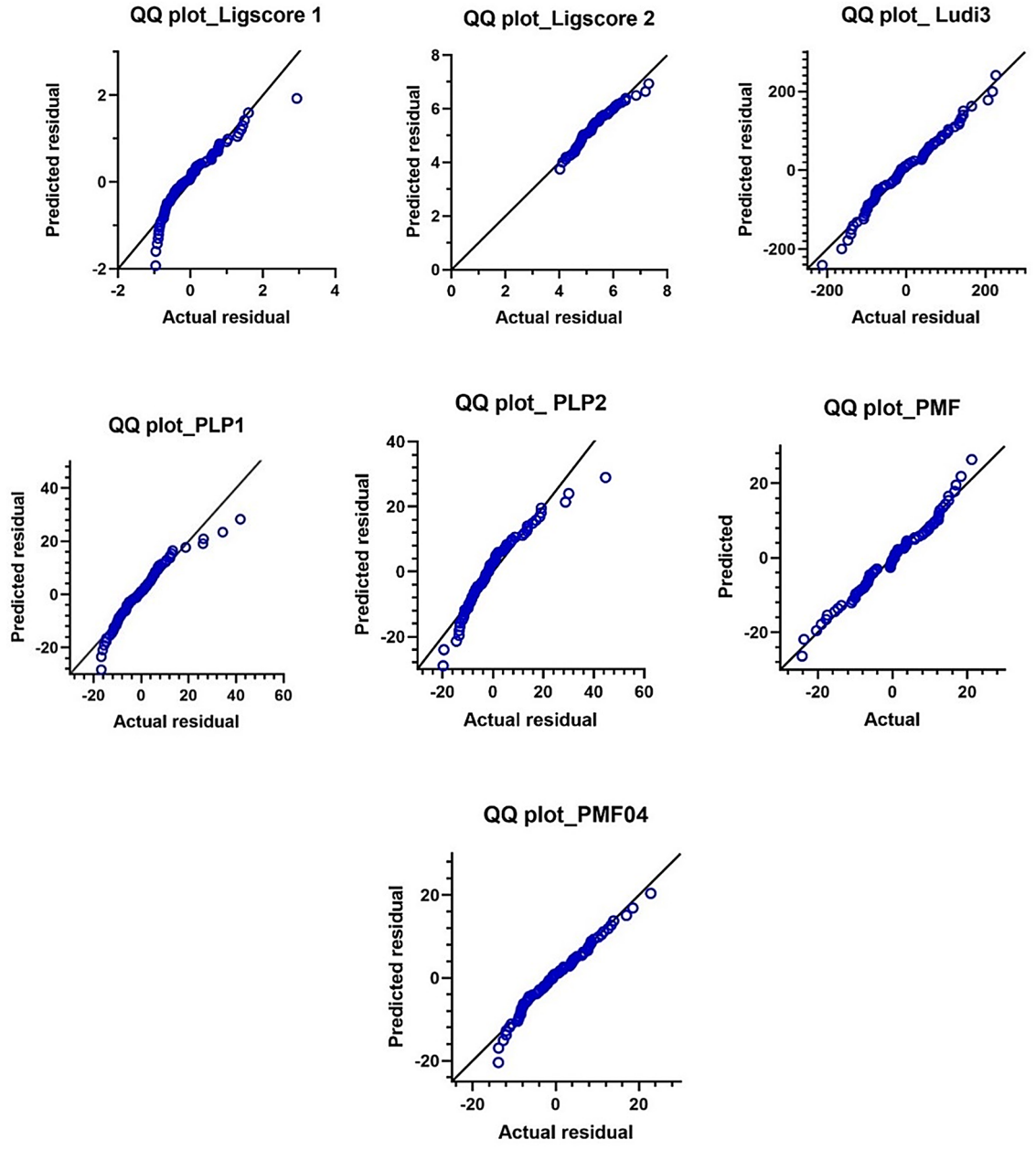

Fig. 5 QQ plot between actual and predicted residual values for calculated scores

non-normality in residuals could have implications for the reliability and the predictive power of these scoring models. Overall, the different scoring functions demonstrated a spectrum of predictiveness and precision. Notably, PMF stood out for its stronger correlation with experimental data, which was evidenced by higher r^2 values, lower mean and standard error of residuals.

Assessment of in silico molecular properties

According to the ligand ID, molecular properties of 73 inhibitors were obtained from PubChem database. Three extra parameters were extracted using DS2019 software: the total count and fractional number of sp^2 hybridized atoms, as well as the total atom count. The data correlation and calculation of the SE values were conducted utilizing the linear regression model in GraphPad Prism software (version 9.3.0.). Detailed parameters of molecular properties could be seen in Table S4. Then, linear correlations between pIC_{50} (pKi) and molecular properties were presented in Table 3 (cf. Fig. S1). Subsequently, QQ plots, similar to those mentioned earlier, were created to examine the predicted versus actual residuals for in silico molecular properties, as illustrated in Fig. S2.

Table 3 Correlation of molecular properties with kinetic data pIC_{50} (pKi) for 73 known inhibitors

Molecular property	Slope*	Y-intercept*	*R* square**	F value	Residuals (D'Agostino-Pearson)	*P* value (D'Agostino-Pearson)
Total number of atoms	6.652 ± 0.831	6.069 ± 5.342	0.475	64.12	12.25	0.002
M W	40.41 ± 6.538	137.4 ± 42.05	0.35	38.2	3.837	0.144
N sp^2 Atoms	2.349 ± 0.285	4.571 ± 1.833	0.489	67.91	5.118	0.077
Fraction sp^2 Atoms	-0.00265 ± 0.0105	0.736 ± 0.068	0.000897	0.064	2.315	0.314
H_donor	0.118 ± 0.073	0.465 ± 0.472	0.035	2.567	3.94	0.139
H_Acceptor	0.495 ± 0.139	1.719 ± 0.891	0.153	12.78	2.979	0.226
R_bonds	0.424 ± 0.171	1.524 ± 1.099	0.08	6.148	10.9	0.004
Complexity	79.52 ± 10.75	94.24 ± 69.14	0.435	54.71	0.194	0.908
Top. Polar Surface Area	6.177 ± 1.967	37.76 ± 12.65	0.122	9.857	0.00994	0.995
Heavy Atom Count	3.497 ± 0.381	5.219 ± 2.449	0.543	84.28	2.474	0.290

*Best-fit value ± SE

**$p < 0.0001$

Higher r^2 values correlated with several key molecular features, including the total number of atoms, the number of sp^2 hybridized atoms, molecular complexity, and the heavy atom count. These parameters were somewhat connected. The total number of atoms encompassed both heavy and hydrogen atoms. Whereas, the number of sp^2 hybridized atoms captured the planar, unsaturated features such as double bonds and aromatic rings, contributing to the molecule's complexity which arose from various structural elements including rings, bonds, and stereochemistry. Together, these factors interplayed to define the molecular size, shape, complexity, and potential reactivity.

The highest correlation was observed in the number of heavy atoms, reflected by an r^2 value exceeding 0.5 and an F statistic near 85. Ranking second in correlation was the number of sp^2 hybridized atoms, with an r^2 value of 0.489, which was slightly outperformed by the number of atoms with an r^2 of 0.475. The results indicated a preference of BRD4 (BD1) for larger ligands, characterized by a higher count of heavy atoms and a significant presence of non-saturated or aromatic bonds. This preference was attributed to the large number of aromatic residues within the BRD4 (BD1) active site, which stabilized ligands through diverse π-π or π-cation interactions. Conversely, the fraction of sp^2 hybridized atoms was unexpectedly the least correlating parameter, with an r^2 value only of 0.000897. This indicated that, although the presence of sp^2 hybridized atoms was advantageous, the overall size or the absolute number of atoms in a ligand was more important. The complexity parameter ($r^2 = 0.435$, $F = 54.71$) showed notable but slightly lower correlation than both the number of heavy atoms and sp^2 hybridized atoms. What's more, molecular weight showed moderate correlation ($r^2 = 0.35$, $F = 38.2$), which was depended on the total number of atoms and was associated with the count of heavy atoms.

Five parameters, including the number of hydrogen bond acceptor, topological polar surface area (TPSA), the number of rotatable bonds (R_bonds) and the number of hydrogen bond donor, yielded an r^2 value below 0.2 despite their significance in assessing ligand druggability. The above introduced fraction of sp^2 hybridized atoms was also included in this study. Specifically, the relative count of hydrogen bond acceptors correlated weakly with the observed data, as evidenced by a low r^2 value of 0.153 ($F = 12.78$). For ligands such as 1M3, U0D and 2TA, the number of hydrogen bond acceptors was identified to be 9, whereas it was found to be only 1 for ligands 15E and RLG. Another parameter TPSA, which measured the polar region on a molecular surface dominated by oxygen and nitrogen, offered insights into the drug-like attributes of a molecule, such as absorption and permeability, thus facilitating pharmacokinetic and drug delivery evaluations. Notably, TPSA showed a modest correlation with an r^2 value of 0.122 ($F = 9.857$). For example, ligand TVU from structure 4UIX exhibited the highest TPSA value of 139 Å, correlating with a moderate pIC_{50} of 7.3, while RLG from structure 6VUB showed a TPSA of 20.3 Å, coinciding with the lowest pIC_{50} of 3.4. Generally, molecules with a TPSA over 140 Å squared displayed poor cell membrane permeation, while those with a TPSA under 90 Å squared were typically necessary for penetration of the blood-brain barrier to affect central nervous system targets.

Molecular interaction analysis

Analysis of protein-ligand interactions also gave insight into how BRD4 (BD1) interacted with inhibitors and provided guidance for the design of new BRD4 (BD1) inhibitors. We selected the top ten compounds ($IC_{50} \leq 15$ nM) for research by using CDOCKER protocol. To do this, ligand coordinates were extracted from their original crystal structures, and re-docked into their corresponding crystal structure of BRD4 (BD1). The binding modes

of the ligands in the crystal structures were shown in Fig. S3 and the interactions were summarized in Table S5. Hydrogen bond, van der Waals interaction, pi-alkyl interaction, and alkyl interaction were observed in all molecules. Some compounds also had pi-pi T shaped or pi-pi stacked interaction, pi-sigma or pi-sulfur interaction, carbon hydrogen bond, water hydrogen bond, and halogen interaction. It was worth noting that the hydrogen bond formed by the ligands with the key amino acid Asn140 could be observed in different PDB entries. The non-bonded interactions between inhibitors and the WPF shelf consisting of Trp81, Pro82 and Phe83 or other ZA channel region were also shown in the interaction diagrams.

Among them, ligand YF2 in crystal structure 6P05 was used as example to detailed analyze its protein-ligand interactions. The 2D and 3D binding interactions between YF2 with BRD4 (BD1) were shown in Fig. 6A and B. The amide moiety of pyrrolopyridone scaffold formed a bidentate hydrogen-bonding interaction with amino acid residue Asn140. And pyrrolopyridone scaffold also formed pi-pi T shaped interaction with Phe83 and Tyr97. The sulfonamide moiety induced a hydrogen-bond network with the ZA loop, involving residues Asp88 and Lys91. The second pyridine ring of YF2 formed pi-alkyl interaction with Leu92 and formed hydrophobic interaction with Leu94. Additional pi-sulfur interaction between the first pyridine ring and Met149 was also observed. Similar to mentioned above, YF2 also had multiple non-bonded interactions with BRD4 (BD1). These interactions were consistent with experimental interaction reported in the literature [37]. Of note, the consistency of the interaction results could also be explained by the re-docked poses. As shown in Fig. 6C, yellow sticks represented the crystallographic pose, and blue sticks represented the redocked pose. The skeleton of YF2 was basically overlapped and a slight deviation in the branched chain was revealed. A low RMSD (0.3266 Å) suggested that the redocked ligand assumed a pose that was very close to its experimentally determined position, pointing towards the reliability of the docking parameters and algorithms used.

MD simulation

To explore the binding stability of inhibitor YF2 to the active site of BRD4 (BD1), the initial docking position of YF2 was set as the starting point for 30 ns MD simulation. Typically, the RMSD of the backbone atoms within a complex was a good indicator of its stability over time. A lower RMSD suggested a more stable system [48]. As depicted in Fig. 7A, both the free protein and BRD4 (BD1)-YF2 complex maintained RMSD values below 0.30 nm during the 30 ns period. Specifically, the RMSD of the free protein system oscillated from 0.15 to 0.225 nm after 15 ns, whereas the RMSD of the BRD4 (BD1)-YF2 complex exhibited fluctuations within the range of 0.15 to 0.25 nm after 11 ns of the simulation. The average RMSD vales for the free protein and BRD4 (BD1)-YF2 systems measured throughout the entire simulation were 0.1896 nm and 0.1901 nm, respectively. These minor fluctuations and the overall low RMSD values suggested that the inhibitor-bound protein backbones remained stable relative to their initial structures.

The RMSF values for the residues in the stabilized systems were then analyzed. The RMSF values signified the extent of variability for each amino acid residue after inhibitor binding. Higher RMSF scores suggested greater fluctuations [49]. Figure 7B showed that the RMSF values for all residues were below 0.30 nm except for the N-terminal and C-terminal of BRD4 (BD1). This suggested that

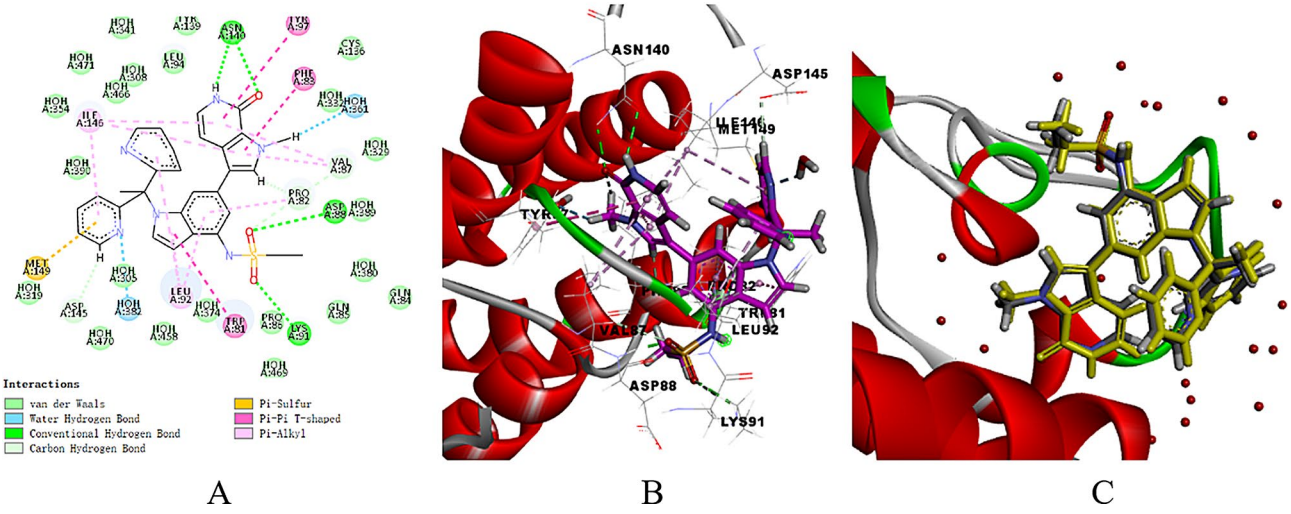

Fig. 6 (**A**) 2D binding mode of BRD4 (BD1) (PDB: 6P05) with inhibitor YF2; (**B**) 3D binding mode of BRD4 (BD1) with inhibitor YF2; (**C**) The CDOCKER docking mode of inhibitor YF2 to BRD4 (BD1). Yellow: the crystallographic pose; Blue: the redocked pose

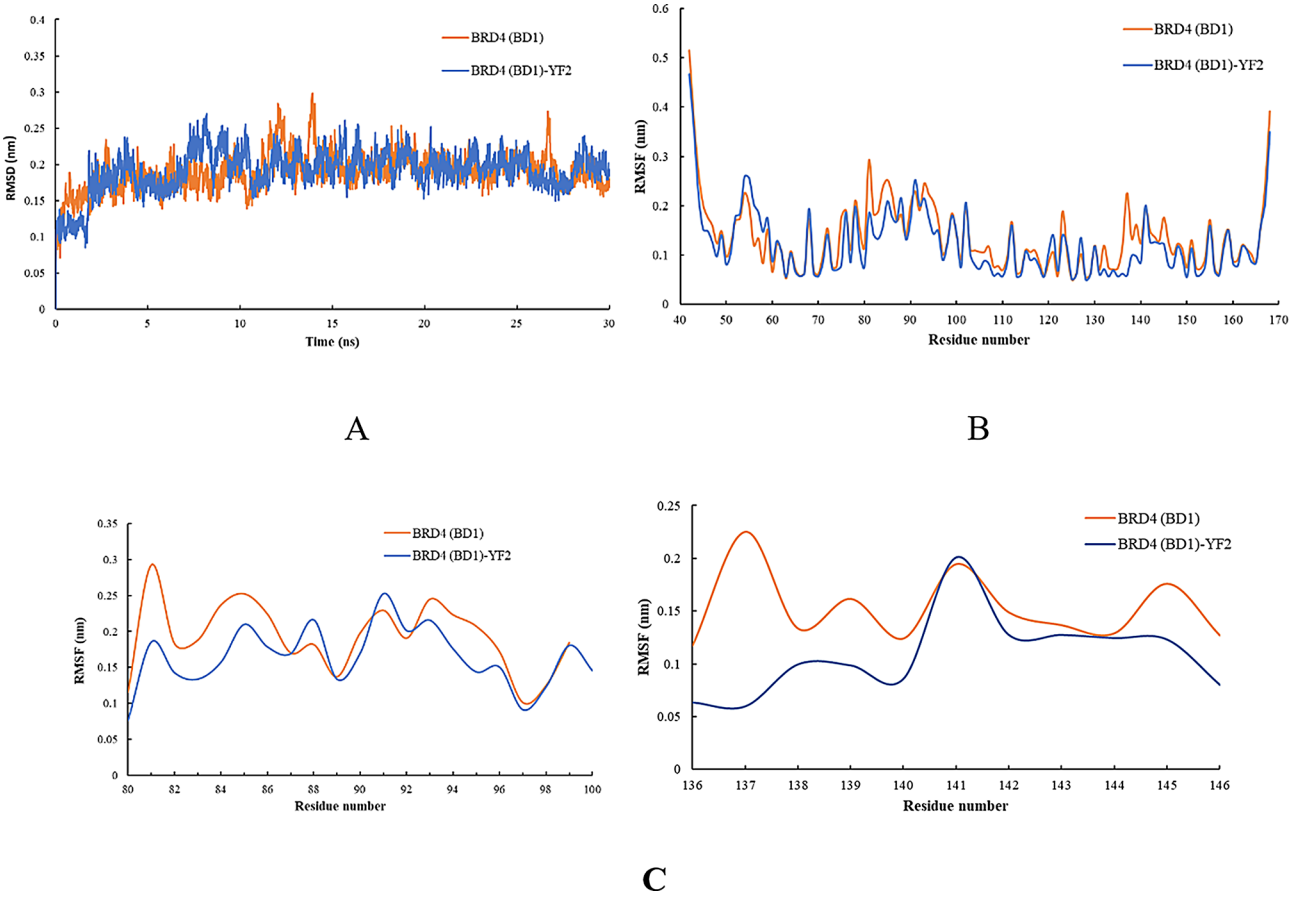

Fig. 7 (**A**) The RMSD plot of backbone atoms; (**B**) The RMSF plot of each residue; (**C**) RMSF plot of the key residues obtained from the full RMSF plot

the proteins within both systems demonstrated a low-flexibility state. The RMSF plot (referenced as Fig. 7C) distinctly illustrated that the key residues (Trp81, Pro82, Phe83, Tyr97, and Asn140) in BRD4 (BD1)-YF2 complex displayed less fluctuation compared to the unbound protein. The results indicated that stable interactions were formed between the protein structure and inhibitor YF2 and aligned with the previous findings from molecular docking studies.

Conclusions

In this study, docking methods, scoring functions and in silico molecular properties were assessed on a test set of 73 BRD4 (BD1) protein-ligand complexes. The CDOCKER protocol, boasting an 86.3% success rate, was the superior choice for BRD4 (BD1) docking, offering high reliability for medium-scale virtual screening for BRD4 (BD1) inhibitors. Correlation analysis between various scoring functions: LigScore1, LigScore2, PLP1, PLP2, PMF, PMF04, and Ludi3 with inhibition constants of ligands identified PMF as the top performer, with an r^2 value of 0.614. These results highlighted the efficacy of scoring functions in docking based virtual screening and deepened understanding of the structure-activity relationships in BRD4 (BD1) drug designing. In silico correlation analysis linked specific molecular properties to BRD4 (BD1) ligand affinity, informing future design strategies. The methodologies introduced in this research held potential for broader application across various macromolecules, facilitating the exploration and development of novel ligands.

Supplementary Information

The online version contains supplementary material available at https://doi.org/10.1186/s13065-024-01362-5.

Supplementary Material 1

Acknowledgements
Not applicable.

Author contributions
J.M. have performed evaluation and validation of docking methods, scoring functions and drafted the manuscript. X.H. outlined the research strategy and revised the manuscript. All authors read and approved the final manuscript.

Funding
This study had no funding support.

Data availability
The datasets used and/or analysed during the current study are available from the corresponding author on reasonable request.

Declarations

Ethics approval and consent to participate
Not applicable.

Consent for publication
Not applicable.

Competing interests
The authors declare no competing interests.

Received: 2 June 2024 / Accepted: 8 December 2024
Published online: 18 December 2024

References

1. Vemula D, Jayasurya P, Sushmitha V, Kumar YN, Bhandari V. CADD, AI and ML in drug discovery: A comprehensive review. Eur J Pharm Sci. 2023;181:106324.
2. Zhang H, Shen C, Zhang HR, Chen WX, Luo QQ, Ding L. Discovery of novel DGAT1 inhibitors by combination of machine learning methods, pharmacophore model and 3D–QSAR model. Mol Divers. 2021;25:1481–95.
3. Sledz P, Caflisch A. Protein structure-based drug design: from docking to molecular dynamics. Curr Opin Struct Biol. 2018;48:93–102.
4. Lin Y, Zhang Y, Wang D, Yang B, Shen YQ. Computer especially AI-assisted drug virtual screening and design in traditional Chinese medicine. Phytomedicine. 2022;107:154481.
5. Crampon K, Giorkallos A, Deldossi M, Baud S, Steffenel A. Machine-learning methods for ligand-protein molecular docking. Drug Discov Today. 2022;27:151–64.
6. Asiamah I, Obiri SA, Tamekloe W, Armah FA, Borquaye LS. Applications of molecular docking in natural products-based drug discovery. Sci Afr. 2023;20:e01593.
7. Solanki P, Rana N, Jha PC, Manhas A. A comprehensive analysis of the role of molecular docking in the development of anticancer agents against the cell cycle CDK enzyme. Biocell. 2023;47:707–29.
8. Rawat S, Subramaniam K, Subramanian SK, Subbarayan S, Dhanabalan S, Chidambaram SKM, Stalin B, Roy A, Nagaprasad N, Aruna M, Tesfaye JL, Badassa B, Krishnaraj R. Drug Repositioning Using Computer-aided Drug Design (CADD). Curr Pharm Biotechnol. 2024;25:301–12.
9. Gahbauer S, DeLeon C, Braz JM, Craik V, Kang HJ, Wan X, Huang X, Billesbølle CB, Liu Y, Che T, Deshpande I, Jewell M, Fink EA, Kondratov IS, Moroz YS, Irwin JJ, Basbaum AI, Roth BL, Shoichet BK. Docking for EP4R antagonists active against inflammatory pain. Nat Commun. 2023;14:8067.
10. Rehman HM, Sajjad M, Ali MA, Gul R, Naveed M, Aslam MS, Shinwari K, Bhinder MA, Ghani MU, Saleem M, Rather MA, Ahmad I, Amin A. Identification of RdRp inhibitors against SARS-CoV-2 through E-pharmacophore-based virtual screening, molecular docking and MD simulations approaches. Int J Biol Macromol. 2023;237:124169.
11. Tran-Nguyen VK, Junaid M, Simeon S, Ballester PJ. A practical guide to machine-learning scoring for structure-based virtual screening. Nat Protoc. 2023;18:3460–511.
12. Li J, Fu A, Zhang L. An overview of scoring functions used for protein-ligand interactions in molecular docking. Interdisciplinary Sciences: Comput Life Sci. 2019;11:320–8.
13. Bender BJ, Gahbauer S, Luttens A, Lyu J, Webb CM, Stein RM, Fink EA, Balius TE, Carlsson J, Irwin JJ, Shoiche BK. A practical guide to large-scale docking. Nat Protoc. 2021;16:4799–832.
14. Cui H, Divakaran A, Hoell ZH, Ellingson MO, Scholtz CR, Zahid H, Johnson JA, Griffith EC, Gee CT, Lee AL, Khanal S, Shi K, Aihara H, Shah VH, Lee RE, Harki DA, Pomerantz WCK. A Structure-based Design Approach for Generating High Affinity BRD4 D1-Selective Chemical Probes. J Med Chem. 2022;65:2342–60.
15. Tang P, Zhang JF, Liu J, Cheng-Ming C, Liang QY. Targeting bromodomain and extraterminal proteins for drug discovery: from current progress to technological development. J Med Chem. 2021;64:2419–35.
16. Feng ZY, Chen AP, Shi J, Zhou DG, Shi W, Qiu QQ, Liu XH, Huang WL, Li JM, Qian H, Zhang WJ. Design, synthesis, and biological activity evaluation of a series of novel sulfonamide derivatives as BRD4 inhibitors against acute myeloid leukemia. Bioorg Chem. 2021;111:104849.
17. He ZX, Jiao HM, An Q, Zhang X, Zengyangzong D, Xu JL, Liu HM, Ma LY, Zhao W. Discovery of novel 4-phenylquinazoline-based BRD4 inhibitors for cardiac fibrosis. Acta Pharm Sin B. 2022;12:291–307.
18. Gupta A, Purohit R. Identification of potent BRD4-BD1 inhibitors using classical and steered molecular dynamics based free energy analysis. J Cell Biochem. 2024;125:e30532.
19. Filippakopoulos P, Qi J, Picaud S, Shen Y, Smith WB, Fedorov O, Morse EM, Keates T, Hickman TT, Felletar I, Philpott M, Munro S, McKeown MR, Wang YC, Christie AL, West N, Cameron MJ, Schwartz B, Heightman TD, Thangue NL, French CA, Wiest O, Kung AL, Knapp S, Bradner JE. Selective inhibition of BET bromodomains. Nature. 2010;468:1067–73.
20. Jiang F, Hu QH, Zhang ZM, Li HM, Li HL, Zhang DW, Li HW, Ma Y, Xu JJ, Chen HF, Cui Y, Zhi YL, Zhang YM, Xu JY, Zhu JP, Lu T, Chen YD. Discovery of Benzo [cd] indol-2 (1H)-ones and Pyrrolo [4,3,2- de] quinolin-2 (1H)-ones as Bromodomain and Extra-Terminal Domain (BET) Inhibitors with Selectivity for the First Bromodomain with Potential High Efficiency against Acute Gouty Arthritis. J Med Chem. 2019;62:11080–107.
21. Gilan O, Rioja I, Knezevic K, Bell MJ, Yeung MM, Harker NR, Lam EYN, Chung CW, Bamborough P, Petretich M, Urh M, Atkinson SJ, Bassil AK, Roberts EJ, Vassiliadis D, Burr ML, Preston AGS, Wellaway C, Werner T, Gray JR, Michon AM, Gobbetti T, Kumar V, Soden PE, Haynes A, Vappiani J, Tough DF, Taylor S, Dawson SJ, Bantscheff M, Lindon M, Drewes G, Demont EH, Daniels DL, Grandi P, Prinjha RK, Dawson MA. Selective targeting of BD1 and BD2 of the BET proteins in cancer and immunoinflammation. Science. 2020;368:387–94.
22. Faivre EJ, McDaniel KF, Albert DH, Mantena SR, Plotnik JP, Wilcox D, Zhang L, Bui MH, Sheppard GS, Wang L, Sehgal V, Lin XY, Huang XL, Lu X, Uziel T, Hessler P, Lam LT, Bellin RJ, Mehta G, Fidanze S, Pratt JK, Liu DC, Hasvold LA, Sun CH, Panchal SC, Nicolette JJ, Fossey SL, Park CH, Longenecker K, Bigelow L, Torrent M, Rosenberg SH, Kati WM, Shen Y. Selective inhibition of the BD2 bromodomain of BET proteins in prostate cancer. Nature. 2020;578:306–10.
23. Ding MY, Shao YY, Sun DW, Meng S, Zang Y, Zhou YB, Li J, Lu W, Zhu SL. Design, synthesis, and biological evaluation of BRD4 degraders. Bioorg Med Chem. 2023;78:117134.
24. Gavai AV, Norris D, Delucca G, Tortolani D, Tokarski JS, Dodd D, O'Malley D, Zhao YF, Quesnelle C, Gill P, Vaccaro W, Huynh T, Ahuja V, Han WC, Mussari C, Harikrishnan L, Kamau M, Poss M, Sheriff S, Yan CH, Marsilio F, Menard K, Wen ML, Rampulla R, Wu DR, Li JQ, Zhang HP, Li P, Sun D, Yip H, Traeger SC, Zhang YR, Mathur A, Zhang HY, Huang C, Yang Z, Ranasinghe A, Everlof G, Raghavan N, Tye CK, Wee S, Hunt JT, Vite G, Westhouse R, Lee FY. Discovery and Preclinical Pharmacology of an Oral Bromodomain and Extra-Terminal (BET) Inhibitor Using Scaffold-Hopping and Structure-Guided Drug Design. J Med Chem. 2021;64:14247–65.
25. Dong J, Wang X. Identification of novel BRD4 inhibitors by pharmacophore screening, molecular docking, and molecular dynamics simulation. J Mol Struct. 2023;1274:134363.
26. Zhong H, Wang X, Chen S, Wang Z, Wang H, Xu L, Hou T, Yao X, Li D, Pan P. Discovery of Novel Inhibitors of BRD4 for Treating Prostate Cancer: A Comprehensive Case Study for Considering Water Networks in Virtual Screening and Drug Design. J Med Chem. 2024;67:138–51.
27. Ibrahim MAA, Abdelhamid MMH, Abdeljawaad KAA, Abdelrahman AHM, Mekhemer GAH, Sidhom PA, Sayed SRM, Paré PW, Hegazy MF, Shoeib T. Pyronaridine as a Bromodomain-Containing Protein 4- N-Terminal Bromodomain (BRD4-BD1) Inhibitor: In Silico Database Mining, Molecular Docking, and Molecular Dynamics Simulation. Molecules. 2023;28:5713.
28. Allen BK, Mehta S, Ember SWJ, Zhu J, Schönbrunn E, Ayad NG, Schürer SC. Identification of a novel class of BRD4 inhibitors by computational screening and binding simulations. ACS Omega. 2017;2:4760–71.
29. Šinko G. Assessment of scoring functions and in silico parameters for AChE-ligand interactions as a tool for predicting inhibition potency. Chemi-Biol Interact. 2019;308:216–23.
30. Berman HM, Westbrook J, Feng Z, Gilliland G, Bhat TN, Weissig H, Shindyalov IN, Bourne PE. The Protein Data Bank. Nucleic Acids Res. 2000;28:235–42.
31. Filippakopoulos P, Picaud S, Mangos M, Keates T, Lambert JP, Barsyte-Lovejoy D, Felletar I, Volkmer R, Muller S, Pawson T, Gingras AC, Arrowsmith CH, Knapp S. Histone recognition and large scale structural analysis of the human bromodomain family. Cell. 2012;149:214–31.

32. Lian X, Xia Z, Li X, Karpov P, Jin H, Tetko IV, Xia J, Wu S. Anti-MRSA drug discovery by ligand-based virtual screening and biological evaluation. Bioorg Chem. 2021;114:105042.
33. Jiang Y, Gao H. Pharmacophore-based drug design for the identification of novel.
34. butyrylcholinesterase inhibitors. against Alzheimer's disease. Phytomedicine. 2019;54:278–90.
35. Ayoub AM, Hawk LML, Herzig RJ, Jiang J, Wisniewski AJ, Gee CT, Zhao P, Zhu JY, Berndt N, Offei-Addo NK, Scott TG, Qi J, Bradner JE, Ward TR, Schönbrunn E, Georg, Pomerantz WCK. BET Bromodomain Inhibitors with One-Step Synthesis Discovered from Virtual Screen. J Med Chem. 2017;60:4805–17.
36. Hou Y, Xie H, Dou G, Yang W, Ge J, Zhou B, Ren J, Li J, Wang J, Zhang Z, Wang X. Computational study on novel natural inhibitors targeting c-MET. Med (Baltim). 2021;100:e27171.
37. Wu G, Robertson DH, Brooks CL 3rd, Vieth M. Detailed analysis of grid-based molecular docking: A case study of CDOCKER-A CHARMm-based MD docking algorithm. J Comput Chem. 2003;24:1549–62.
38. Li Y, Zhao J, Gutgesell LM, Shen Z, Ratia K, Dye K, Dubrovskyi O, Zhao H, Huang F, Tonetti DA, Thatcher GRJ, Xiong R. Novel Pyrrolopyridone Bromodomain and Extra-Terminal Motif (BET) Inhibitors Effective in Endocrine-Resistant ER + Breast Cancer with Acquired Resistance to Fulvestrant and Palbociclib. J Med Chem. 2020;63:7186–210.
39. Picaud S, Da Costa D, Thanasopoulou A, Filippakopoulos P, Fish PV, Philpott M, Fedorov O, Brennan P, Bunnage ME, Owen DR, Bradner JE, Taniere P, O'Sullivan B, Muller S, Schwaller J, Stankovic T, Knapp S. PFI-1, a highly selective protein interaction inhibitor, targeting BET Bromodomains. Cancer Res. 2013;73:3336–46.
40. Guest EE, Pickettb SD, Hirst JD. Structural variation of protein–ligand complexes of the first bromodomain of BRD4. Org Biomol Chem. 2021;19:5632.
41. Li YF, Zhao J, Gutgesell LM, Shen Z, Ratia K, Dye K, Dubrovskyi O, Zhao H, Huang F, Tonetti DA, Thatcher GRJ, Xiong R. Novel Pyrrolopyridone Bromodomain and Extra-Terminal Motif (BET) Inhibitors Effective in Endocrine-Resistant ER + Breast Cancer with Acquired Resistance to Fulvestrant and Palbociclib. J Med Chem. 2020;63:7186–210.
42. Feng Z, Chen A, Shi J, Zhou D, Shi W, Qiu Q, Liu X, Huang W, Li J, Qian H, Zhang W. Design, synthesis, and biological activity evaluation of a series of novel sulfonamide derivatives as BRD4 inhibitors against acute myeloid leukemia. Bioorg Chem. 2021;111:104849.
43. Wang S, Jiang JH, Li RY, Deng P. Docking–based virtual screening of TβR1 inhibitors: evaluation of pose prediction and scoring functions. BMC Chem. 2020;14:52.
44. Kim S, Chen J, Cheng T, Gindulyte A, He J, He S, Li Q, Shoemaker BA, Thiessen PA, Yu B, Zaslavsky L, Zhang J, Bolton EE. PubChem in 2021: new data content and improved web interfaces. Nucleic Acids Res. 2021;49:D1388–95.
45. Hess B, Kutzner C, van der Spoel D, Lindahl E. GROMACS 4: algorithms for highly efficient, load-balanced, and scalable molecular simulation. J Chem Theory Comput. 2008;4:435–47.
46. Yu YL, Krämer A, Venable RM, Simmonett AC, MacKerell AD Jr, Klauda JB, Pastor RW, Brooks BR. Semi-automated optimization of the CHARMM36 lipid force field to include explicit treatment of long-range dispersion. J Chem Theory Comput. 2021;17:1562–80.
47. Bussi G, Donadio D, Parrinello M. Canonical sampling through velocity rescaling. J Chem Phys. 2007;126:014101.
48. Chen XZ, Yu XY, Dai C, Huang QY, Shen Y, Wang J, Hu Y, Lin ZH. Identification of potent CypD inhibitors via pharmacophore based virtual screening, docking and molecular dynamics simulation. J Mol Struct. 2022;1247:131355.
49. Yu D, Du J, He P, Wang N, Li L, Liu Y, Yang C, Xu H, Li Y. Identification of natural xanthine oxidase inhibitors: Virtual screening, anti-xanthine oxidase activity, and interaction mechanism. Int J Biol Macromol. 2024;259:129286.

Publisher's note